



Supplementary Information for

## Spatiotemporal dissociation of fMRI activity in the caudate nucleus underlies human *de novo* motor skill learning

**Short Title:** Spatiotemporal dissociation in the caudate nucleus

**Authors:** Yera Choi<sup>1,4</sup>, Emily Yunha Shin<sup>1,4</sup>, Sungshin Kim<sup>1,2,3\*</sup>

1. Center for Neuroscience Imaging Research, Institute for Basic Science, Suwon 16419, Republic of Korea
2. Sungkyunkwan University, Suwon 16419, Republic of Korea
3. Department of Cognitive Sciences, Hanyang University, Seoul 04763, Republic of Korea
4. These authors equally contributed to this study

\*Corresponding Author

N Center Suite 86363, Sungkyunkwan University,  
2066 Seobu-ro, Jangan-gu,  
Suwon, Gyeonggi-do, Republic of Korea  
+82-10-4687-5322  
sungshin0207@gmail.com

### This PDF file includes:

- SI Methods
- Figures S1 to S11
- Tables S1 to S4
- A legend for Movie S1
- SI References

### Other supplementary materials for this manuscript include the following:

- Movie S1

## SI Methods

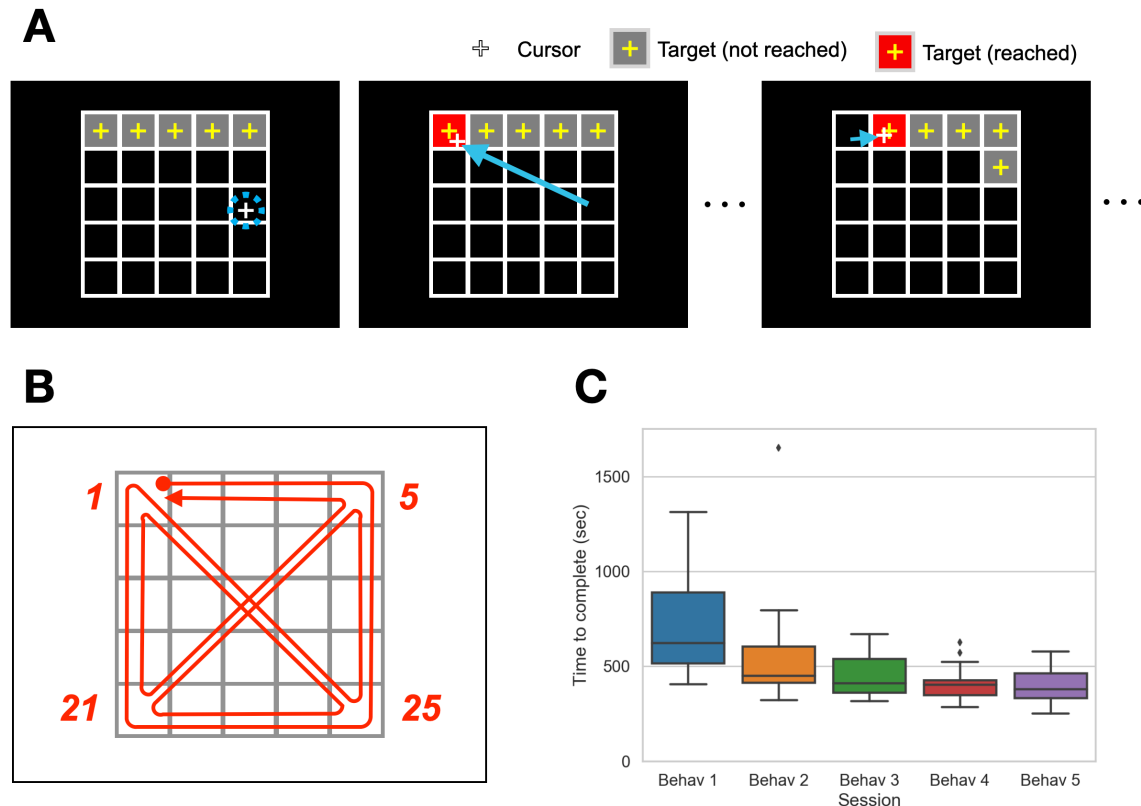
**Manual extraction of the caudate nucleus.** To explore the distinct functional characteristics of the subregions of the caudate nucleus, we separated the caudate nucleus into three parts, head, body, and tail. Accurate delineation of the caudate tail is particularly difficult due to its narrow, curved, and obscured structure, which makes it inherently vulnerable to partial volume effects (1). Accordingly, the extremity of the caudate tail is frequently excluded from both atlas-defined and automatically segmented ROIs (1).

To better account for the problems regarding delineation as well as for individual variations in the caudate structure, we performed manual segmentation to create individual ROIs for the caudate nucleus. Manual segmentation for all participants was performed by one research trainee (S.Y.L.) using ITK-SNAP version 3.8.0 (2), with the guidance of researchers well experienced with MRI data processing and manual segmentation (H.F.K., H.J.K.). The boundaries of the caudate subregions were chosen based on previous literature (1, 3-5). In each hemisphere, the caudate head ROI started from the region superior to the nucleus accumbens and extended along with the anterior horn of the lateral ventricle, until it reached the vertical line traversing the anterior commissure (VAC) on the sagittal plane; the caudate body ROI, which continued to extend along the region superior to the body of the lateral ventricle, was bounded between the VAC and the vertical line traversing the posterior commissure (VPC) on the sagittal plane; the caudate tail ROI was defined as the region extending from the VPC back toward the anterior. To generate more even and continuous ROIs, additional postprocessing steps including small island removal (removing islands smaller than ten voxels) and smoothing (filling sharp corners and holes smaller than a kernel size of 3 mm) were performed using 3dSlicer version 4.10.2 (<https://www.slicer.org/>) (6).

As manual segmentation is also not free from the issue of partial volume effects, a separate set of caudate ROIs was created using the Reinforcement Learning Atlas (7), which provides high-resolution delineations of subcortical structures including the caudate tail. This set of ROIs was used for group analyses and visualization. The atlas-defined ROIs presented high similarity with the group average of manually segmented ROIs. Specifically, at the image intensity of 0.3 (an arbitrary threshold to maximize the similarity between the numbers of voxels contained by the manually segmented and corresponding atlas-defined ROIs), the group average of the combined manually segmented ROIs (663 voxels) and the combined atlas-defined ROI (662 voxels) demonstrated 61% overlap of selected voxels. All created ROIs were resampled using AFNI's *3dresample* function to the participants' EPI dimensions (2.683 mm<sup>3</sup> isotropic voxels).

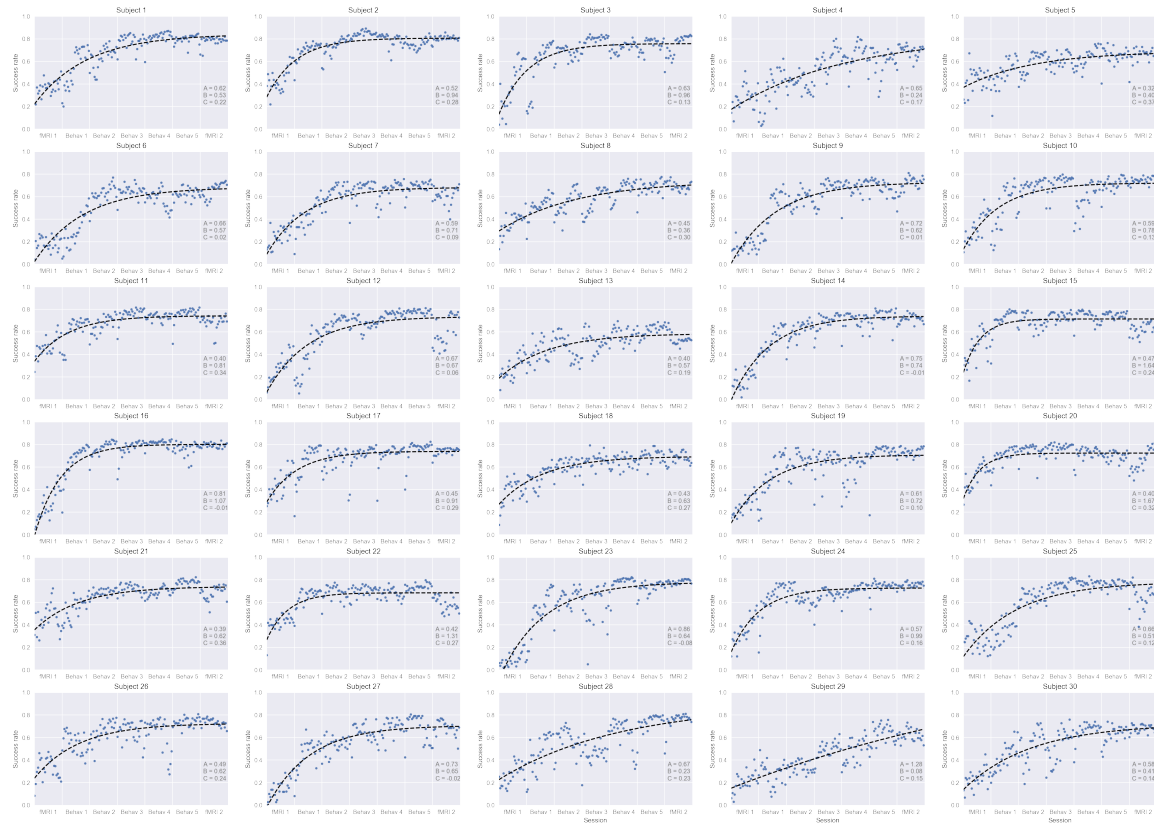
**Transfer of learning.** We examined the extent of transfer of learning between the trained and untrained mappings through the following procedure (Fig. S3B). First, as a measure of the amount of learning, the time-varying change in the success rate for each mapping in each fMRI session was obtained by subtracting the success rate of the first-block from those of the subsequent blocks. Thus, the overall learned amount was measured in the last block (marked with a red arrow in Fig. S3A and shown as a bar graph in Fig. S3B). The *initial* amount of transfer was calculated as the difference between the learned amount in the *first session* of the trained mapping (i.e., the first three trained-mapping runs of the first fMRI) from that for the untrained mapping (i.e., the three untrained-mapping runs of the first fMRI). Similarly, the *final* amount of transfer was calculated as the difference between the learned amounts in the *second respective sessions* of the trained (i.e., the three trained-mapping main-task runs of the first behavioral training) and untrained mappings (i.e., the three untrained-mapping runs of the second fMRI). In addition, to examine the amount of saving or relearning, we calculated the within-mapping differences in the learned amount, by comparing the first and second sessions of each mapping. We used a non-parametric test instead of a *t*-test due to the violation of normality identified in the initial transfer of learning.

**Fig. S1. Path-following task**



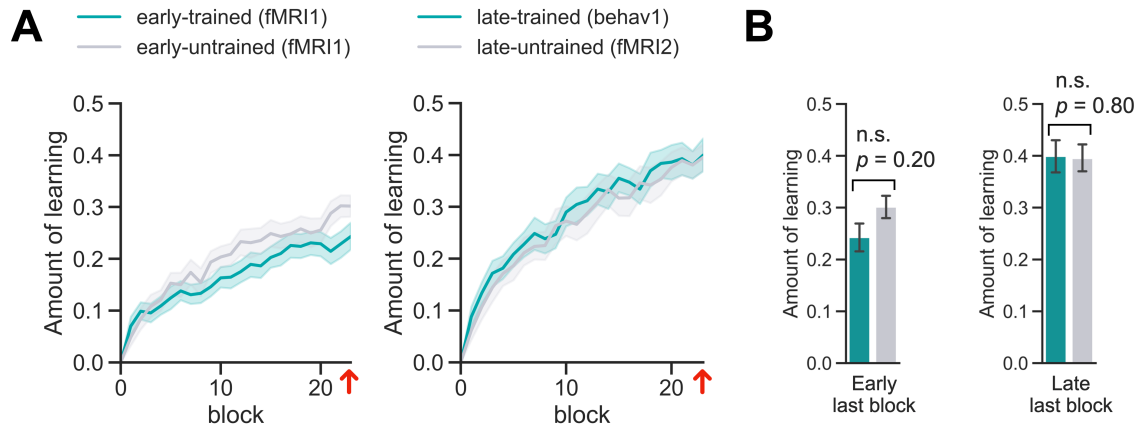
Overview of the path-following task that was presented in the last two runs of the five behavioral training sessions. This task was introduced to facilitate the generalized learning of the mapping between the cursor position and hand posture, which would be not restricted to the cognitive and discrete knowledge of the hand postures corresponding to the four corner targets in the main task. **A.** In the path-following task, one target and four upcoming targets indicating the path to follow were shown. When the participants stably reached the current target or failed to reach it at all within 5 s, the target was moved to the next target specified in the predetermined sequence (shown in **B**). As the goal of the task was to reach the targets as soon and accurately as possible, straighter movements along the path were encouraged. **B.** The full sequence of targets in each path-following block is depicted in red. The circle denotes the starting point and the arrowhead denotes the endpoint. **C.** The total time taken by individual participants to complete the path-following runs in each behavioral session is represented by each boxplot. Evidently, the time to complete significantly decreased from the first to the fifth behavioral session ( $p < 10^{-5}$ , Wilcoxon signed-rank test).

**Fig. S2. Individual learning performance for the trained mapping across all sessions**



The individual success rate curves from all participants ( $n = 30$ ). For the calculation of the individual learning rate, an exponential model with three parameters ( $A, B, C$ ) was fitted to the block-by-block success rate for the trained mapping for all fMRI and behavioral training sessions, with the following equation:  $S(t) = A(1 - e^{-Bt}) + C$ , where  $t$  denotes learning blocks, and  $B$  denotes the learning rate. For each plot, the three parameters,  $A$ ,  $B$ , and  $C$ , are shown in the bottom right. Black solid lines denote the fitted exponential models. Blue dots indicate the actually observed block-by-block (consisting of 12 repetitive trials) success rates. The 29th participant was excluded as an outlier in the resting state fMRI functional connectivity analysis due to exceptionally low performance during the behavioral training sessions (lower 0.3% in the distribution of the overall success rates). The estimated learning rate of the outlier was also very low (0.076), compared with other participants (second-lowest = 0.23).

**Fig. S3. Assessment of transfer of learning**

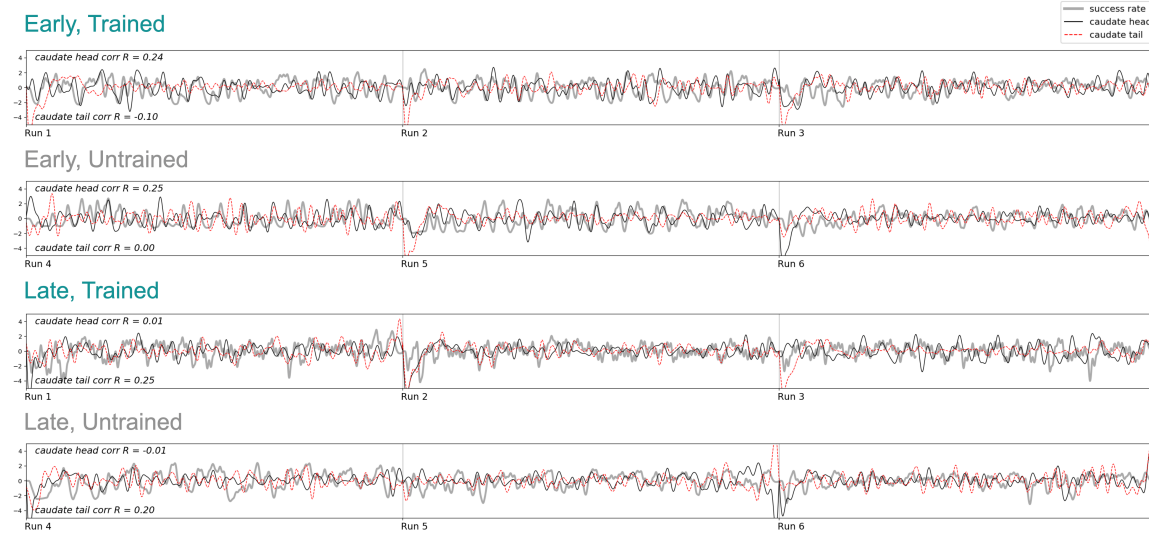


**A.** Line plots representing the block-by-block amounts of learning for the trained (green) and untrained (gray) mappings. The left panel shows the values from the first respective sessions of the two mappings (“early-trained”: the first three trained-mapping runs of the first fMRI; “early-untrained”: the three untrained-mapping runs of the first fMRI). The right panel presents the values from the second respective sessions of the mappings (“late-trained”: the three trained-mapping main-task runs of the first behavioral training; “late-untrained”: the three untrained-mapping runs of the second fMRI). Lighter-colored shades around the solid lines indicate SE. The red arrow in each panel indicates the last block (Block 24). For detailed information on the procedures to calculate the amounts of learning, see SI Methods.

**B.** Bar graphs depicting the amount of learning in the last block for each mapping. The left panel presents the comparison between the first respective sessions of the two mappings (“early-trained”: green; “early-untrained”: gray). The right panel shows the comparison between the second respective sessions of the two mappings (“late-trained”: green; “late-untrained”: gray). We found the learned amounts for the mappings significantly increased from the first to second respective sessions (trained mapping:  $p < 10^{-3}$ , untrained mapping:  $p < 0.01$ ), which reflect savings (faster relearning) (8, 9). Neither the first ( $p = 0.20$ ) nor second session ( $p = 0.80$ ) showed significant within-stage differences between mappings. All comparisons were performed using Wilcoxon signed-rank tests to account for the violation of normality, and uncorrected  $p$  values are presented. Error bars indicate SE.

Abbreviations: SE, standard error.

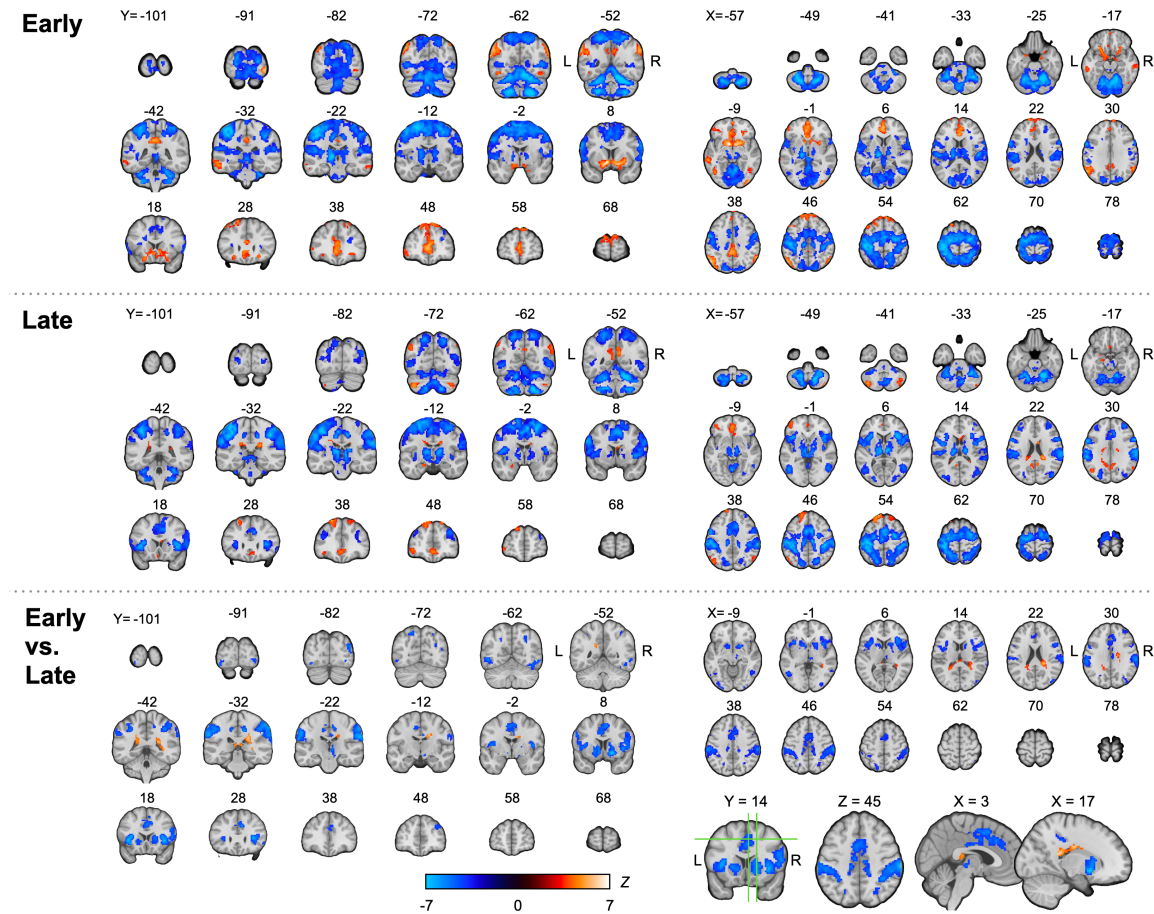
**Fig. S4. Example time-series plots of HRF-convolved time-varying success rate and fMRI activities in the caudate head and tail from a representative participant**



The time-series plots of the HRF-convolved time-varying success rate for the trained mapping (solid gray line) and the fMRI activities in the caudate head (solid black line) and tail (red dotted line) from a representative subject (Subject 2; with the highest overall success rate of 0.73). The success-modulated fMRI activities were extracted from the peak voxels in each run according to the following criteria. For the early stage, the positive peak of the caudate head and the negative peak of the caudate tail were selected. For the late stage, the negative peak of the caudate head and the positive peak of the caudate tail were chosen. In each panel, the zero-lag correlation coefficients ( $R$ ) between the convolved success rate and the fMRI activities at the peak voxels (head: top left corner; tail: bottom left corner) are listed. The complete results from all participants are shown in Figure S11.

Abbreviations: fMRI, functional magnetic resonance imaging; HRF, hemodynamic response function; MNI, Montreal Neurological Institute; ROI, region of interest.

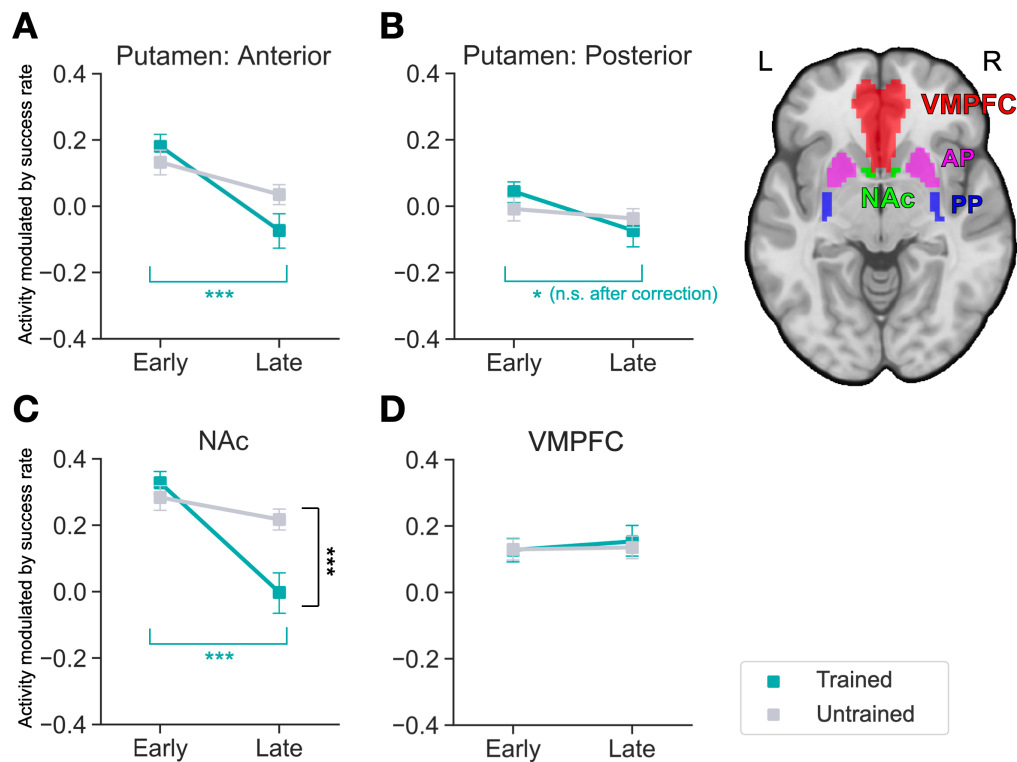
**Fig. S5. Whole-brain voxel-wise GLM analyses contrasting the early and late stages of learning (Late – Early)**



Regions significantly modulated by the success rate in the first (“Early”) and second (“Late”) fMRI sessions were identified based on whole-brain voxel-wise GLM analyses. In the “Early” and “Late” panels, the red-orange continuum indicates the regions that showed significant *positive* modulation, while the blue-light blue continuum indicates the regions that showed significant *negative* modulation. The most regions showing the negative success-rate modulation are related to motor execution (M1/S1, SMA, super- and inferior-parietal lobules, Cerebellum) due to our experiment design in which participants tended to move less with a higher success rate ( $R = -0.70 \pm 0.01$ , mean  $\pm$  SE). In the “Early vs. Late” panel, the red-orange continuum denotes the regions that showed significant *increases* in success-modulated fMRI activities, while the blue-light blue continuum denotes the regions that showed significant *decreases* in success-modulated fMRI activities, from Early to Late stage of learning. The right bottom section of the “Early vs. Late” panel presents four slices containing regions of particular interest, including the regions with increased (posterior caudate nucleus) and decreased activities (supramarginal gyrus, middle cingulate cortex, insula, superior parietal cortex, anterior putamen, and anterior caudate nucleus). The color bar indicates the group-level Z-scores, and numbers above each slice indicate MNI coordinates.

Abbreviations: M1, primary motor cortex; S1, primary somatosensory cortex; SMA, supplementary motor area; GLM, general linear model; L, left; MNI, Montreal Neurological Institute; R, right.

**Fig. S6. Locations of the selected ROIs implicated in reward processing**

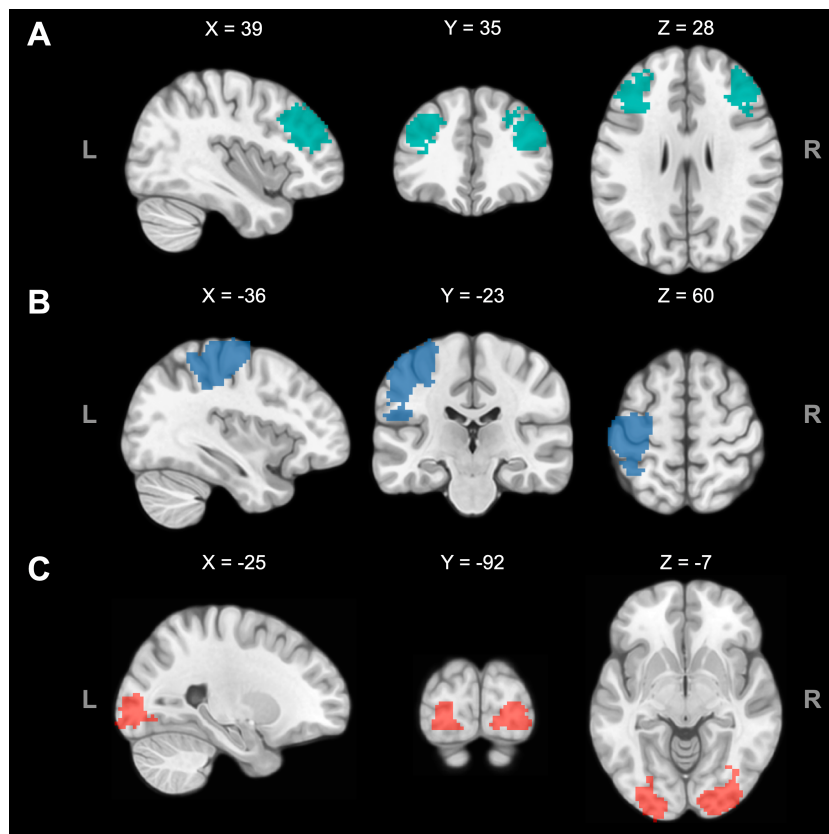


In addition to the three ROIs in the caudate nucleus (results shown in Figure 4), four cortical and subcortical ROIs implicated in reward processing were included in the ROI analyses to examine potential changes in success-modulating fMRI activity from the early to late stage of learning. These non-caudate ROIs included: **A**. anterior putamen (AP); **B**. posterior putamen (PP); **C**. nucleus accumbens (NAc); **D**. ventromedial prefrontal cortex (VMPFC). For each ROI, activity modulated by the time-varying success rate for the trained (solid green line) and untrained (solid gray line) mappings in the early and later stages of learning are shown in panels **A-D**. Error bars indicate SE. The respective locations of these ROIs are shown in the upper right panel.

Uncorrected  $p$ : \* $, p < 0.05$ ; \*\* $, p < 0.01$ ; \*\*\* $, p < 0.001$ ; n.s., not significant.

Abbreviations: AP, anterior putamen; NAc, nucleus accumbens; PP, posterior putamen; ROI, region of interest; SE, standard error; VMPFC, ventromedial prefrontal cortex.

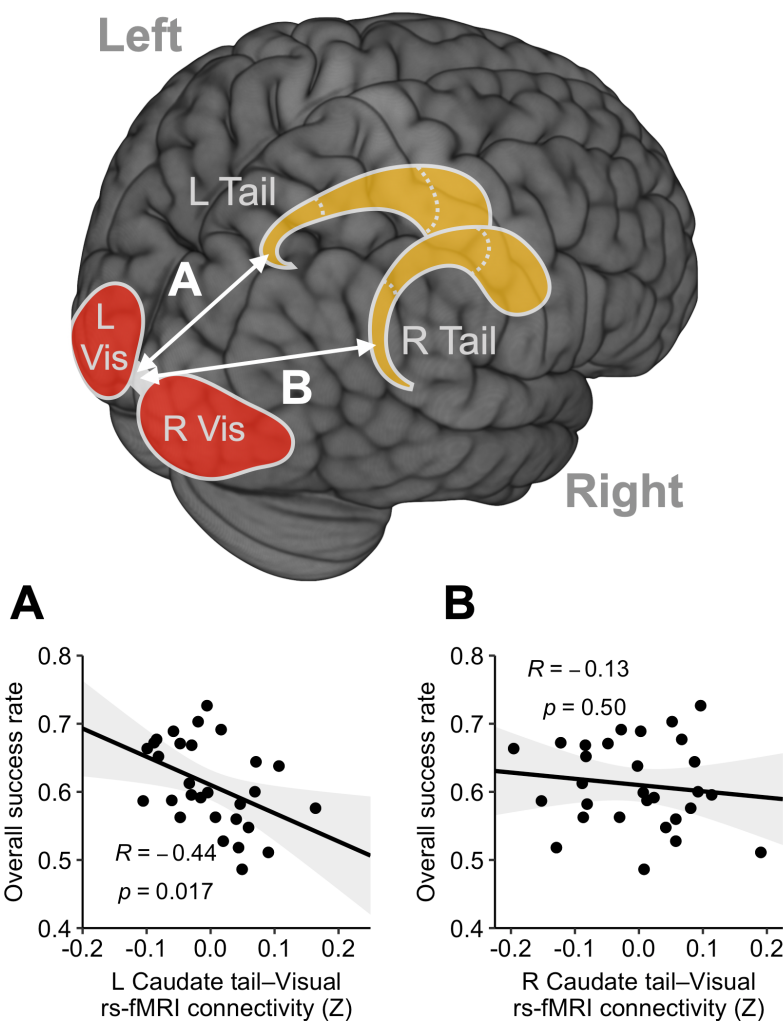
**Fig. S7. Locations of the independently defined ROIs encompassing the left/right DLPFC and left M1/S1**



**A.** The cortical ROI of the DLPFC (L: 717 voxels; R: 767 voxels) was obtained from the Neurosynth database (on September 23, 2019), with the use of the term “dorsolateral prefrontal” which retrieved 1049 studies and 36216 activations. **B.** The ROI encompassing the left M1/S1 (1330 voxels) was defined by using the data from an independent localizer scan, which identified the regions selectively activated by random movements of right fingers (Table S4). **C.** The ROI encompassing the bilateral visual areas (L: 326 voxels, R: 477 voxels) were defined by using the data from the trained-mapping of the second fMRI (“Late” stage). The XYZ coordinates are in the MNI space.

Abbreviations: DLPFC, dorsolateral prefrontal cortex; L, left; MNI, Montreal Neurological Institute; M1, primary motor cortex; R, right; ROI, region of interest; S1, primary somatosensory cortex.

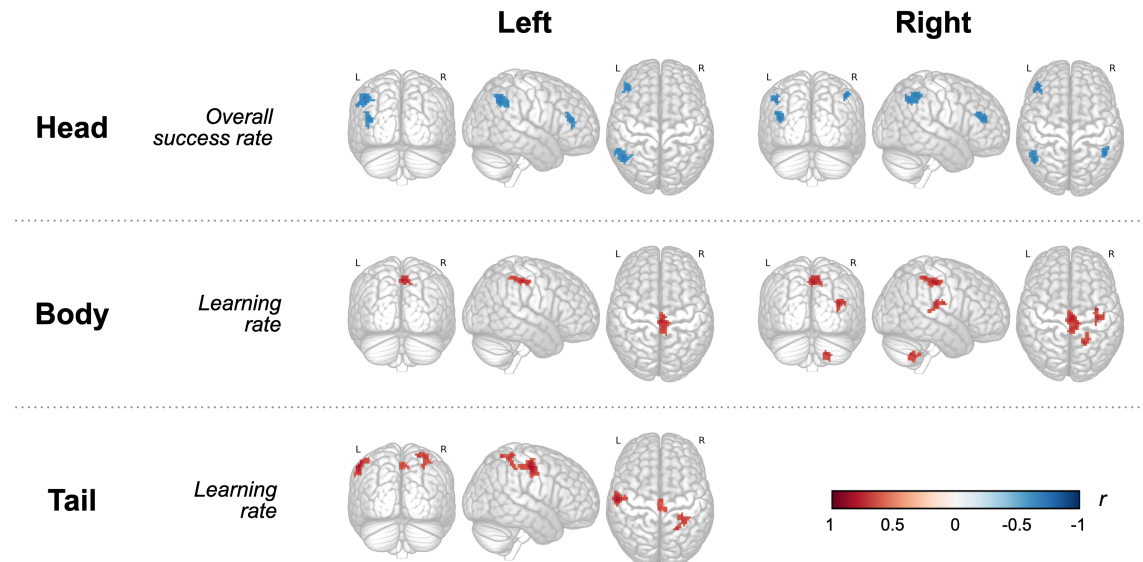
**Fig. S8. Resting-state fMRI connectivity between the caudate tail and visual regions predictive of individual learning performance**



A schematic view of the seed ROI (caudate tail, yellow) and the independently defined cortical ROIs in the bilateral visual region (red). The relationships between the cortico-caudate intrinsic functional connectivity and the overall success rate are shown in bottom panels: **A.** L caudate tail — visual region; **B.** R caudate tail — visual region. The gray shades indicate 95% confidence interval. Pearson correlation coefficients ( $r$ ) and uncorrected  $p$ -values are presented.

Abbreviations: L, left; R, right; Vis, visual region.

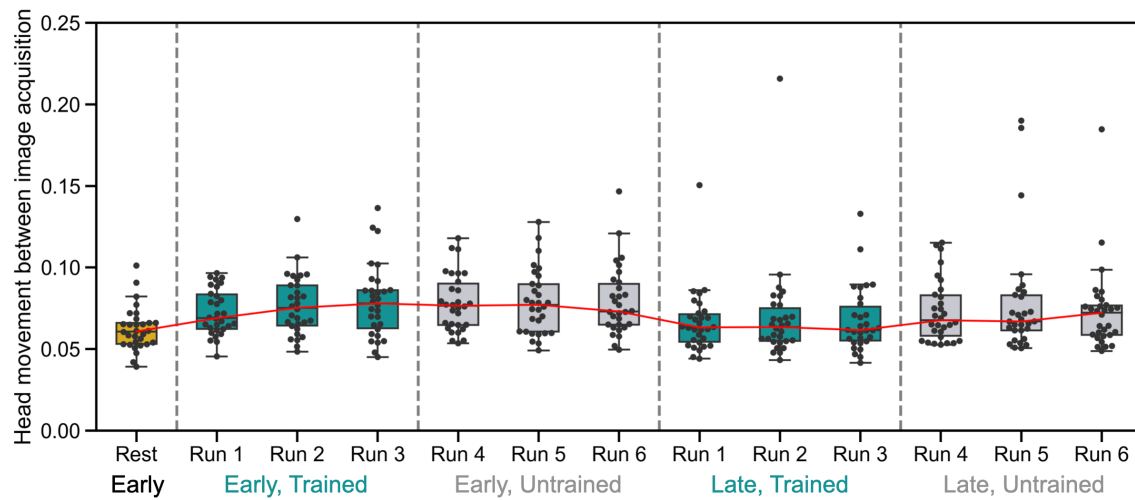
**Fig. S9. Results from exploratory whole-brain connectivity correlation analysis**



Glass-brain demonstration of the exploratory correlation analysis between the whole-brain resting-state connectivity (caudate head/body/tail as seed ROIs) and measures of performance (overall success rate and learning rate). The results were thresholded at voxel-wise  $p < 10^{-3}$ , cluster-wise corrected  $p < 0.05$  (40 voxels). Seed-measure pairs with significant results only are shown. The column “Left” presents the results from the ROIs in the left hemisphere, while the column “Right” shows those from the ROIs in the right hemisphere. Detailed information on the significant clusters is described in Table S3. The color bar indicates Pearson correlation coefficients ( $r$ ). Notably, this figure does not show a significant cluster in the left M1/S1 for the left caudate tail for the overall success rate, although a significant relationship is reported in Fig. 5. This may be due to our application of strict multiple comparison corrections accounting for all voxels in the whole brain. Indeed, with a more lenient threshold of voxel-wise  $p < 0.005$ , we have found a positive cluster with 78 voxels that seems to corroborate our main findings from the hypothesis-driven ROI analysis.

Abbreviations: ROI, region of interest.

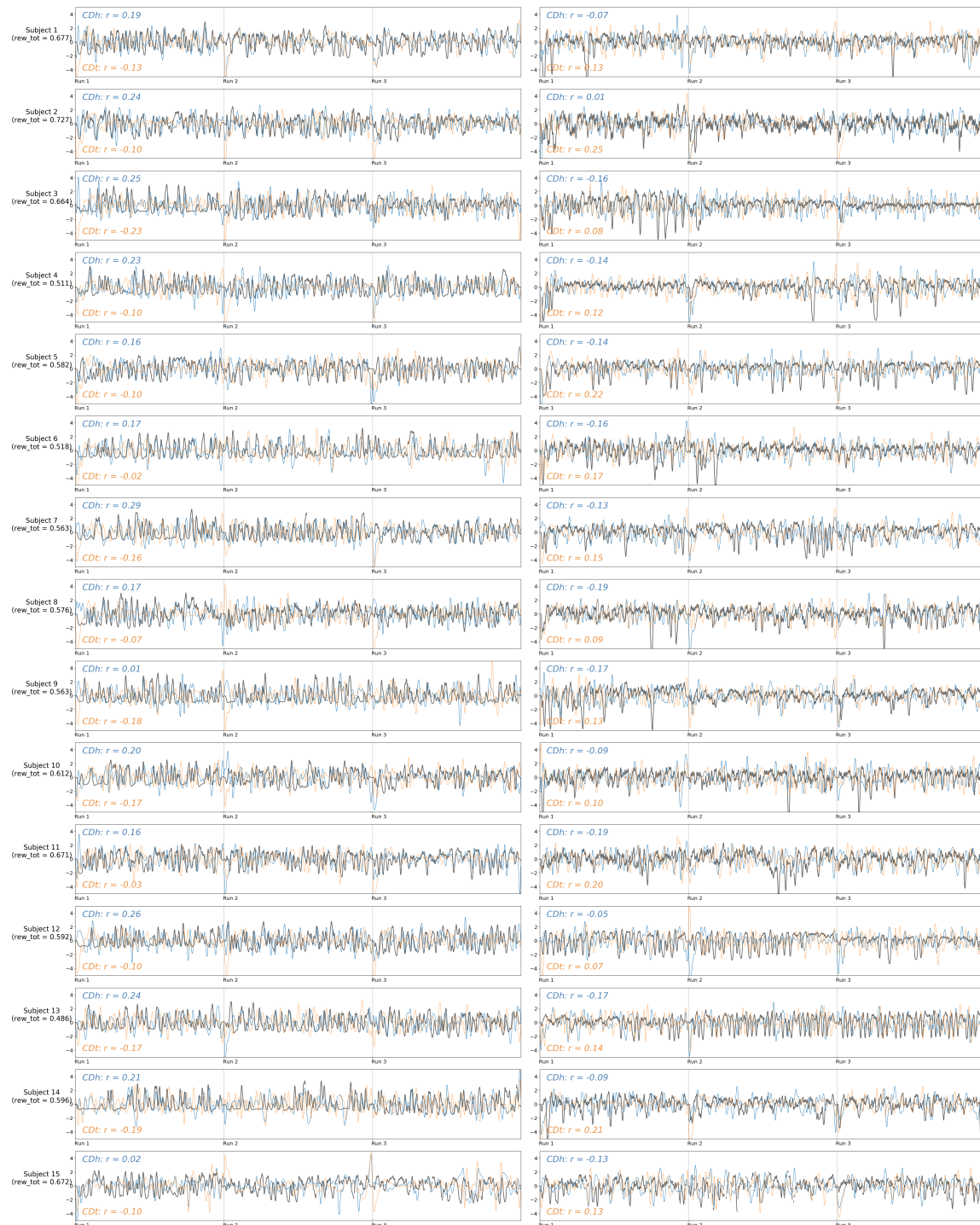
**Fig. S10. Head motion displacement in resting-state and task-based fMRI runs.**

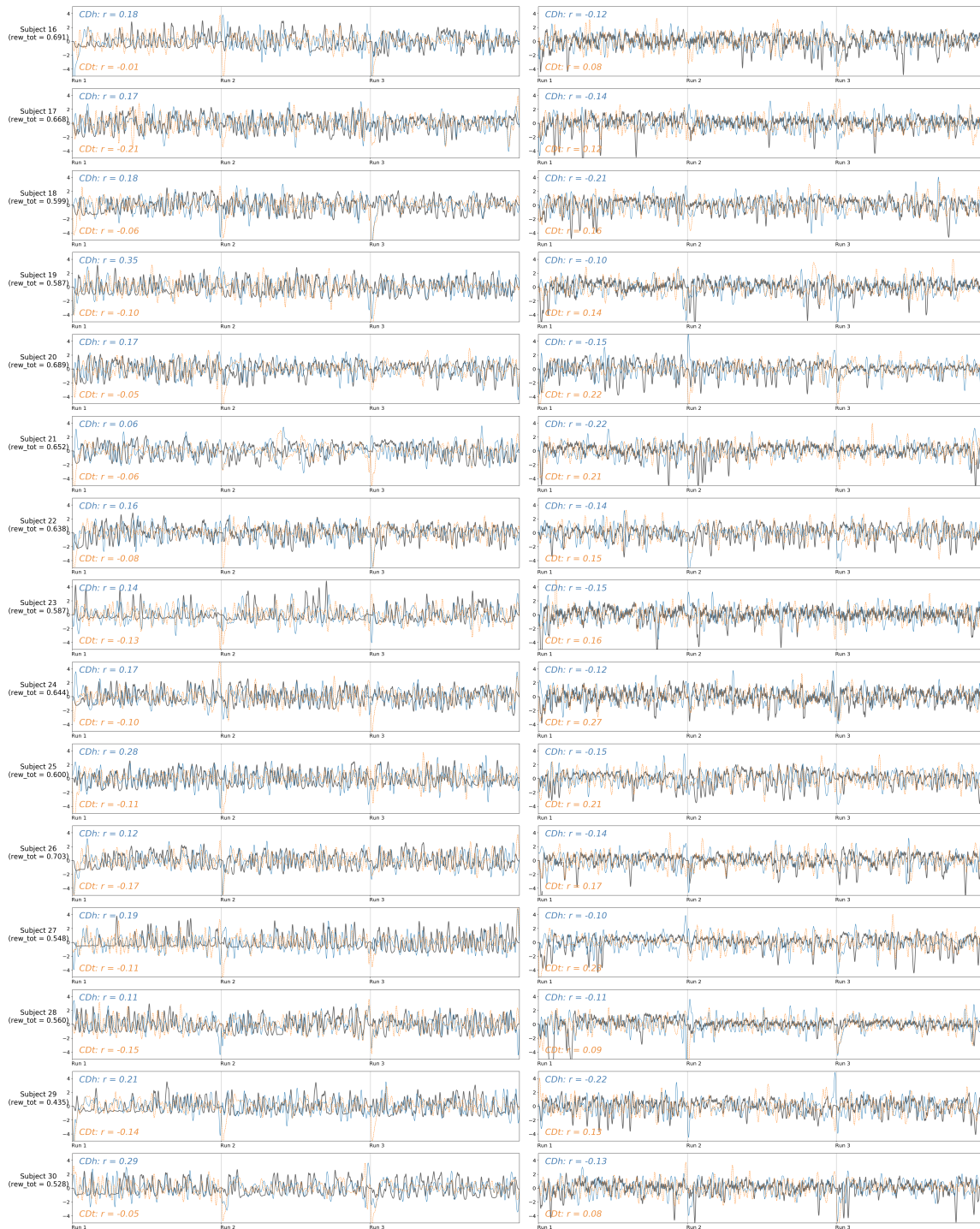


Box plots showing the average amount of displacement (mm) due to head motion, in the resting-state and task-based fMRI runs: (i) “**Rest**”: resting-state fMRI (yellow box); (ii) “**Early**”: first task-based fMRI; (iii) “**Late**”: second task-based fMRI. The runs conducted with the trained (green boxes) and untrained (gray boxes) mappings are noted. The red line indicates the trend of the group median value for each run. The black dots represent individual participants.

**Fig. S11. Time-series correlation between the fMRI activities in the caudate head/tail and HRF-convolved time-varying success rate**

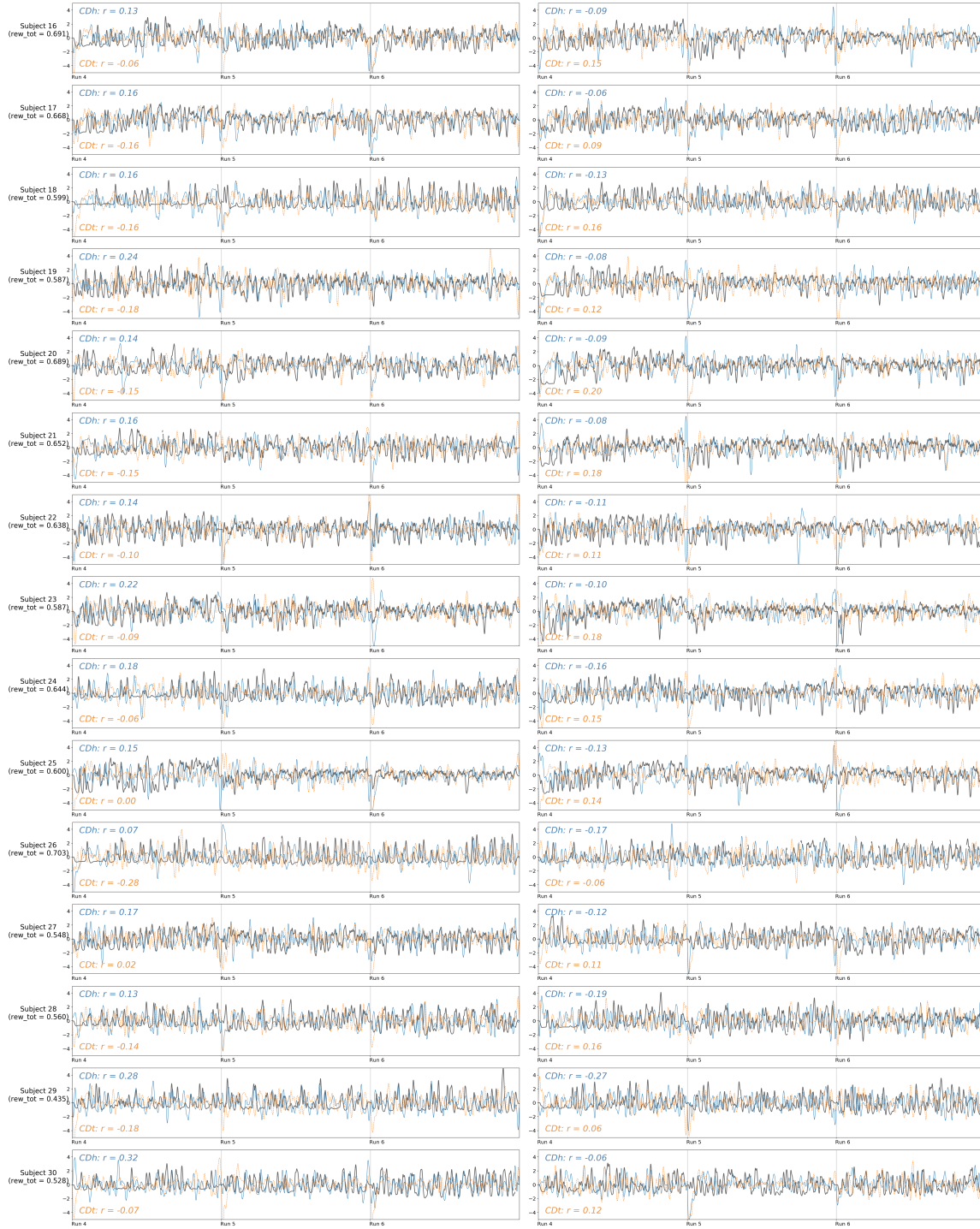
(a) Trained mapping





**(b) Untrained mapping**





The time-series plots of the HRF-convolved time-varying success rate for the trained mapping (black) and the fMRI activities in the caudate head (blue) and tail (orange), from all 30 participants. Each row indicates the data from an individual participant (left column: early stage; right column: late stage). The success-modulated fMRI activities were extracted from the peak voxels in each run, according to the following criteria. For the early stage, the positive peak of the caudate head and the negative peak of the caudate tail were selected. For the late stage, the negative peak of the caudate head and the positive peak of the caudate tail were chosen. In each

panel, the zero-lag correlation coefficients ( $R$ ) between the convolved success rate and the fMRI activities at the peak voxels are listed (head: top left corner; tail: bottom left corner).

Abbreviations: fMRI, functional magnetic resonance imaging; HRF, hemodynamic response function; MNI, Montreal Neurological Institute; ROI, region of interest; CDh, caudate head; CDt, caudate tail; rew\_tot, overall success rate.

**Table S1. Whole-brain voxel-wise GLM analysis comparing the strength of success-rate modulation between early versus late stages of learning**

|                                       | Peak (MNI) |     |     | Cluster size<br>(voxels) | Z-score<br>at peak | Corrected<br><i>p</i> -value |
|---------------------------------------|------------|-----|-----|--------------------------|--------------------|------------------------------|
|                                       | X          | Y   | Z   |                          |                    |                              |
| <b>Early &gt; Late</b>                |            |     |     |                          |                    |                              |
| <i>R Supramarginal Gyrus</i>          | 63         | -26 | 41  | 1059                     | 6.17               | <i>p</i> < 0.01              |
| <i>R Middle Cingulate Cortex</i>      | 9          | 25  | 33  | 878                      | 5.33               | <i>p</i> < 0.01              |
|                                       | 12         | -31 | 41  | 102                      | 4.96               | <i>p</i> < 0.01              |
| <i>R Insula Lobe</i>                  | 36         | 17  | 1   | 818                      | 6.09               | <i>p</i> < 0.01              |
| <i>L Supramarginal Gyrus</i>          | -66        | -26 | 38  | 793                      | 5.84               | <i>p</i> < 0.01              |
| <i>L Insula Lobe</i>                  | -36        | 20  | -5  | 469                      | 5.80               | <i>p</i> < 0.01              |
| <i>R Putamen and Caudate</i>          | 17         | 9   | -7  | 284                      | 6.29               | <i>p</i> < 0.01              |
| <i>L Putamen and Caudate</i>          | -9         | 9   | -8  | 211                      | 5.21               | <i>p</i> < 0.01              |
| <i>R Inferior Temporal Gyrus</i>      | 47         | -56 | -16 | 147                      | 4.70               | <i>p</i> < 0.01              |
| <i>L Middle Temporal Gyrus</i>        | -50        | -58 | -2  | 116                      | 4.73               | <i>p</i> < 0.01              |
| <i>R Middle Occipital Gyrus</i>       | 44         | 82  | 25  | 102                      | 5.03               | <i>p</i> < 0.01              |
| <i>L Superior Parietal Lobule</i>     | -17        | -74 | 54  | 95                       | 4.53               | <i>p</i> < 0.01              |
| <i>L Inferior Occipital Gyrus</i>     | -31        | -99 | -10 | 63                       | 5.23               | <i>p</i> < 0.02              |
| <i>R Thalamus</i>                     | 7          | -23 | 1   | 53                       | 4.56               | <i>p</i> < 0.03              |
| <i>R Angular Gyrus</i>                | 28         | -61 | 43  | 44                       | 3.85               | <i>p</i> < 0.04              |
| <i>R Inferior Occipital Gyrus</i>     | 36         | -88 | -5  | 43                       | 4.33               | <i>p</i> < 0.05              |
| <i>R Middle Frontal Gyrus</i>         | 34         | 49  | 33  | 43                       | 4.27               | <i>p</i> < 0.05              |
|                                       | 47         | 46  | 6   | 41                       | 4.18               | <i>p</i> < 0.05              |
| <i>R Superior Parietal Lobule</i>     | 17         | -72 | 54  | 40                       | 3.86               | <i>p</i> < 0.05              |
| <b>Early &lt; Late</b>                |            |     |     |                          |                    |                              |
| <i>R Caudate</i>                      | 20         | -40 | 19  | 254                      | 5.93               | <i>p</i> < 0.01              |
| <i>L Caudate</i>                      | -26        | -50 | 14  | 97                       | 4.64               | <i>p</i> < 0.01              |
| <i>L Thalamus</i>                     | -4         | -29 | 11  | 43                       | 4.25               | <i>p</i> < 0.05              |
| <b>Common</b>                         |            |     |     |                          |                    |                              |
| <i>Ventromedial Prefrontal Cortex</i> | -4         | 49  | 3   | 138                      | 4.73               | <i>p</i> < 0.01              |
| <i>L Inferior Parietal Lobule</i>     | -50        | -74 | 41  | 124                      | 5.26               | <i>p</i> < 0.01              |
| <i>L Superior Frontal Gyrus</i>       | -9         | 54  | 49  | 108                      | 4.65               | <i>p</i> < 0.01              |
| <i>R Inferior Parietal Lobule</i>     | 58         | -58 | 35  | 55                       | 4.59               | <i>p</i> < 0.05              |
| <i>R Superior Medial Gyrus</i>        | 4          | 52  | 52  | 50                       | 4.25               | <i>p</i> < 0.05              |

Clusters (voxel faces touched) showing significant changes in the modulatory effects of the success rate (“Early > Late”: regions showing decreases; “Early < Late”: regions showing increases) are listed (voxel-wise *p* < 10<sup>-3</sup>, 40 suprathreshold voxels for a cluster-wise corrected *p*

$< 0.05$ ). In addition, the clusters that were significant in both stages (voxel-wise  $p < 10^{-3}$ ,  $> 40$  voxels) were identified as the common regions (“Common”). The average peak Z-scores across learning stages are presented for the common regions.

Abbreviations: L, left; MNI, Montreal Neurological Institute; R, right.

**Table S2. Whole-brain voxel-wise GLM analysis on success-rate modulation in early and late stages of learning, with both positive and negative clusters**

| #                               | Anatomical regions                    | Peak (MNI) |     |     | Cluster size<br>(voxels) | Z-score<br>at peak | Corrected<br><i>p</i> -value |
|---------------------------------|---------------------------------------|------------|-----|-----|--------------------------|--------------------|------------------------------|
|                                 |                                       | X          | Y   | Z   |                          |                    |                              |
| <b>Early, positive clusters</b> |                                       |            |     |     |                          |                    |                              |
| 1                               | <i>L Nucleus Accumbens</i>            | -9         | 6   | -10 | 2355                     | 7.39               | <i>p</i> < 0.01              |
|                                 | <i>Ventromedial Prefrontal Cortex</i> |            |     |     |                          |                    |                              |
|                                 | <i>Putamen and Caudate</i>            |            |     |     |                          |                    |                              |
| 2                               | <i>L Angular Gyrus</i>                | -55        | -66 | 38  | 455                      | 6.26               | <i>p</i> < 0.01              |
| 3                               | <i>L Precuneus</i>                    | -7         | -45 | 38  | 330                      | 5.33               | <i>p</i> < 0.01              |
|                                 | <i>Middle Cingulate Cortex</i>        |            |     |     |                          |                    |                              |
| 4                               | <i>R Angular Gyrus</i>                | 58         | -56 | 33  | 179                      | 5.44               | <i>p</i> < 0.01              |
| 5                               | <i>L Middle Temporal Gyrus</i>        | -63        | -34 | -10 | 172                      | 5.27               | <i>p</i> < 0.01              |
| 6                               | <i>R Inferior Occipital Gyrus</i>     | 36         | -93 | -5  | 85                       | 6.13               | <i>p</i> < 0.01              |
| 7                               | <i>L Inferior Frontal Gyrus</i>       | -47        | 44  | -10 | 76                       | 4.26               | <i>p</i> < 0.02              |
| 8                               | <i>R Inferior Temporal Gyrus</i>      | 47         | -58 | -13 | 64                       | 4.50               | <i>p</i> < 0.02              |
| 9                               | <i>R Middle Temporal Gyrus</i>        | 58         | -26 | -16 | 51                       | 4.18               | <i>p</i> < 0.03              |
| 10                              | <i>L Middle Frontal Gyrus</i>         | -39        | 25  | 49  | 51                       | 4.46               | <i>p</i> < 0.03              |
| 11                              | <i>L Inferior Temporal Gyrus</i>      | -47        | -61 | -13 | 41                       | 4.58               | <i>p</i> < 0.05              |
| <b>Early, negative clusters</b> |                                       |            |     |     |                          |                    |                              |
| 1                               | <i>L Precentral Gyrus</i>             | -44        | -23 | 60  | 25905                    | -8.61              | <i>p</i> < 0.01              |
|                                 | <i>Postcentral Gyrus</i>              |            |     |     |                          |                    |                              |
|                                 | <i>SMA</i>                            |            |     |     |                          |                    |                              |
|                                 | <i>Cerebellum</i>                     |            |     |     |                          |                    |                              |
|                                 | <i>Superior Parietal Lobule</i>       |            |     |     |                          |                    |                              |
|                                 | <i>Inferior Parietal Lobule</i>       |            |     |     |                          |                    |                              |
|                                 | <i>Thalamus</i>                       |            |     |     |                          |                    |                              |
|                                 | <i>Supramarginal Gyrus</i>            |            |     |     |                          |                    |                              |
| 2                               | <i>R Middle Frontal Gyrus</i>         | 31         | 52  | 35  | 131                      | -4.83              | <i>p</i> < 0.01              |
| 3                               | <i>L Caudate, anterior division</i>   | -20        | 9   | 25  | 70                       | -4.69              | <i>p</i> < 0.02              |
| 4                               | <i>R Insula Lobe</i>                  | 36         | 20  | 9   | 55                       | -4.09              | <i>p</i> < 0.03              |
| 5                               | <i>L Insula Lobe</i>                  | -31        | 22  | 9   | 50                       | -4.33              | <i>p</i> < 0.04              |
| <b>Late, positive clusters</b>  |                                       |            |     |     |                          |                    |                              |
| 1                               | <i>L Superior Frontal Gyrus</i>       | -23        | 36  | 57  | 284                      | 5.62               | <i>p</i> < 0.01              |
| 2                               | <i>L Precuneus</i>                    | -20        | -34 | 25  | 255                      | 4.91               | <i>p</i> < 0.01              |

|                                |                                       |     |     |     |       |       |                    |
|--------------------------------|---------------------------------------|-----|-----|-----|-------|-------|--------------------|
| 3                              | <i>Ventromedial Prefrontal Cortex</i> | -1  | 44  | -10 | 240   | 4.78  | <i>p &lt; 0.01</i> |
| 4                              | <i>L Angular Gyrus</i>                | -50 | -74 | 41  | 150   | 4.69  | <i>p &lt; 0.01</i> |
| 5                              | <i>L Middle Frontal Gyrus</i>         | -44 | 54  | -2  | 105   | 4.40  | <i>p &lt; 0.01</i> |
| 6                              | <i>L Cerebellum Crus II</i>           | -39 | -74 | -45 | 92    | 5.13  | <i>p &lt; 0.01</i> |
| 7                              | <i>R Cerebellum Crus II</i>           | 44  | -77 | -37 | 91    | 4.58  | <i>p &lt; 0.01</i> |
| 8                              | <i>R Caudate, posterior division</i>  | 23  | -37 | 22  | 91    | 5.40  | <i>p &lt; 0.01</i> |
| 9                              | <i>R Superior Frontal Gyrus</i>       | 17  | 46  | 52  | 80    | 4.50  | <i>p &lt; 0.02</i> |
| 10                             | <i>R Angular Gyrus</i>                | 58  | -61 | 35  | 78    | 4.34  | <i>p &lt; 0.02</i> |
| 11                             | <i>R Corpus Callosum</i>              | 7   | 9   | 19  | 47    | 4.60  | <i>p &lt; 0.04</i> |
| 12                             | <i>L Caudate, posterior division</i>  | -12 | -18 | 25  | 43    | 4.16  | <i>p &lt; 0.05</i> |
| 13                             | <i>L Hippocampus</i>                  | -20 | -13 | -21 | 42    | 4.20  | <i>p &lt; 0.05</i> |
| <hr/>                          |                                       |     |     |     |       |       |                    |
| <b>Late, negative clusters</b> |                                       |     |     |     |       |       |                    |
| 1                              | <i>L Precentral Gyrus</i>             | -39 | -23 | 52  | 14416 | -7.85 | <i>p &lt; 0.01</i> |
|                                | <i>Postcentral Gyrus</i>              |     |     |     |       |       |                    |
|                                | <i>Superior Parietal Lobule</i>       |     |     |     |       |       |                    |
|                                | <i>SMA</i>                            |     |     |     |       |       |                    |
|                                | <i>Inferior Parietal Lobule</i>       |     |     |     |       |       |                    |
|                                | <i>Insula Lobe</i>                    |     |     |     |       |       |                    |
| 2                              | <i>R Cerebellum</i>                   | 15  | -64 | -50 | 4223  | -7.63 | <i>p &lt; 0.01</i> |
| 3                              | <i>Thalamus and Caudate</i>           | 7   | -18 | 6   | 1586  | -7.23 | <i>p &lt; 0.01</i> |
| 4                              | <i>R Middle Temporal Gyrus</i>        | 44  | -80 | 25  | 735   | -5.48 | <i>p &lt; 0.01</i> |
| 5                              | <i>R Middle Frontal Gyrus</i>         | 34  | 49  | 33  | 283   | -5.73 | <i>p &lt; 0.01</i> |
| 6                              | <i>L Middle Frontal Gyrus</i>         | -44 | 44  | 22  | 165   | -4.60 | <i>p &lt; 0.01</i> |
| 7                              | <i>Brain Stem</i>                     | -1  | -37 | -32 | 112   | -5.12 | <i>p &lt; 0.01</i> |
| 8                              | <i>R Insula Lobe</i>                  | 39  | -10 | -5  | 54    | -5.25 | <i>p &lt; 0.03</i> |

Abbreviations: L, left; MNI, Montreal Neurological Institute; R, right; SMA, supplementary motor area.

**Table S3. Results from the whole-brain connectivity correlation analyses**

|   | Peak (MNI) |     |     | Cluster size | <i>r</i> coefficient |
|---|------------|-----|-----|--------------|----------------------|
|   | X          | Y   | Z   | (voxels)     | at peak              |
| <b>L/R caudate head, learning rate</b>        |            |     |     |              |                      |
| <i>None</i>                                   |            |     |     |              |                      |
| <b>L caudate head, overall success rate</b>   |            |     |     |              |                      |
| <i>L Inferior Parietal Lobule</i>             | -47        | -56 | 41  | 130          | -0.72                |
| <i>L Middle Frontal Gyrus</i>                 | -42        | 38  | 17  | 55           | -0.69                |
| <b>R caudate head, overall success rate</b>   |            |     |     |              |                      |
| <i>L Middle Frontal Gyrus</i>                 | -44        | 44  | 19  | 68           | -0.71                |
| <i>L Inferior Parietal Lobule</i>             | -50        | -58 | 44  | 66           | -0.68                |
| <i>R Inferior Parietal Lobule</i>             | 47         | -50 | 52  | 46           | -0.73                |
| <b>L caudate body, learning rate</b>          |            |     |     |              |                      |
| <i>R Supplementary Motor Area</i>             | 4          | -26 | 52  | 101          | 0.81                 |
| <b>R caudate body, learning rate</b>          |            |     |     |              |                      |
| <i>R Supplementary Motor Area</i>             | 4          | -21 | 49  | 151          | 0.80                 |
| <i>R Insula</i>                               | 36         | -10 | 22  | 72           | 0.77                 |
| <i>R Cerebellum Lobule VIII</i>               | 20         | -56 | -48 | 55           | 0.76                 |
| <b>L/R caudate body, overall success rate</b> |            |     |     |              |                      |
| <i>None</i>                                   |            |     |     |              |                      |
| <b>L caudate tail, learning rate</b>          |            |     |     |              |                      |
| <i>L Postcentral gyrus</i>                    | -58        | -15 | 52  | 108          | 0.83                 |
| <i>R Postcentral gyrus</i>                    | 31         | -42 | 65  | 84           | 0.70                 |
| <i>R Supplementary Motor Area</i>             | 1          | -15 | 54  | 45           | 0.68                 |
| <b>R caudate tail, learning rate</b>          |            |     |     |              |                      |
| <i>None</i>                                   |            |     |     |              |                      |
| <b>L/R caudate tail, overall success rate</b> |            |     |     |              |                      |
| <i>None</i>                                   |            |     |     |              |                      |

The whole-brain connectivity correlation analyses were conducted using two different measures of performance, (i) overall success rate and (ii) learning rate.

Abbreviations: L, left; MNI, Montreal Neurological Institute; R, right.

**Table S4. Clusters showing activity significantly correlated with random finger movements**

|                                   | Peak (MNI) |     |     | Cluster size | Z-score |
|-----------------------------------|------------|-----|-----|--------------|---------|
|                                   | X          | Y   | Z   | (voxels)     | at peak |
| <i>L Pre/Postcentral Gyrus</i>    | -42        | -23 | 60  | 1330         | 13.00   |
| <i>R Cerebellum, Lobules IV-V</i> | 15         | -53 | -26 | 500          | 13.00   |
| <i>R Postcentral Gyrus</i>        | 47         | -26 | 46  | 338          | 6.22    |
| <i>L Posterior Putamen</i>        | -31        | -7  | -2  | 331          | 6.44    |
| <i>R SMA</i>                      | 7          | -2  | 57  | 268          | 6.14    |
| <i>R Cerebellum, Lobule VIII</i>  | 20         | -61 | -53 | 204          | 7.23    |
| <i>L Thalamus</i>                 | -15        | -23 | 3   | 175          | 6.51    |

Note: For robust localization of the region, a highly stringent level of significance (voxel-wise  $p < 10^{-5}$ ) was used.

Abbreviations: L, left; MNI, Montreal Neurological Institute; R, right; SMA, supplementary motor area.

### **Movie S1. Demonstration of finger movements and corresponding cursor movements**

Sample demonstration of finger movements and corresponding cursor movements while performing the main task of the current experiment. The data for the demonstration were acquired independently from an individual (H.K.) who did not participate in the study. The large panel at the center features the two-dimensional space for the cursor movement, while the small panel at the bottom right corner shows the corresponding right finger movements. The movie presents two different sets of movements (Movements 1 and 2) to reach the targets in the four corner cells as in the main task, demonstrating multiple hand postures can be implemented to reach the same target.

## SI References

1. J. C. L. Looi *et al.*, Volumetrics of the caudate nucleus: Reliability and validity of a new manual tracing protocol. *Psychiatry Research: Neuroimaging* **163**, 279-288 (2008).
2. P. A. Yushkevich *et al.*, User-guided 3D active contour segmentation of anatomical structures: Significantly improved efficiency and reliability. *NeuroImage* **31**, 1116-1128 (2006).
3. H. Hokama *et al.*, Caudate, putamen, and globus pallidus volume in schizophrenia: A quantitative MRI study. *Psychiatry Research: Neuroimaging* **61**, 209-229 (1995).
4. D. E. Haines, G. A. Mihailoff, "Chapter 16 - The Telencephalon" in Fundamental Neuroscience for Basic and Clinical Applications (Fifth Edition), D. E. Haines, G. A. Mihailoff, Eds. (Elsevier, 2018), <https://doi.org/10.1016/B978-0-323-39632-5.00016-5>, pp. 225-240.e221.
5. C. A. Seger, The visual corticostriatal loop through the tail of the caudate: circuitry and function. *Front Syst Neurosci* **7**, 104 (2013).
6. A. Fedorov *et al.*, 3D Slicer as an image computing platform for the Quantitative Imaging Network. *Magn Reson Imaging* **30**, 1323-1341 (2012).
7. W. M. Pauli, A. N. Nili, J. M. Tyszka, A high-resolution probabilistic in vivo atlas of human subcortical brain nuclei. *Scientific Data* **5**, 180063 (2018).
8. V. S. Huang, A. Haith, P. Mazzoni, J. W. Krakauer, Rethinking motor learning and savings in adaptation paradigms: model-free memory for successful actions combines with internal models. *Neuron* **70**, 787-801 (2011).
9. M. A. Smith, A. Ghazizadeh, R. Shadmehr, Interacting adaptive processes with different timescales underlie short-term motor learning. *PLoS biology* **4**, e179 (2006).